ELSEVIER

Journal of Nuclear Materials 306 (2002) 112–120

journal of nuclear materials

www.elsevier.com/locate/jnucmat

Effect of sputtering in Xe ion irradiated yttria-stabilized zirconia

I.V. Afanasyev-Charkin, K.E. Sickafus *

Materials Science and Technology Division, Los Alamos National Laboratory, MS-G755, Los Alamos, NM 87545, USA

Received 19 March 2002; accepted 7 September 2002

Abstract

Fully stabilized zirconia is known as a radiation resistant material. The objective of many experiments on zirconia has been to test the susceptibility of this material to amorphization. Because zirconia exhibits high radiation tolerance, this has made very high fluence ion irradiation experiments a necessity and so, additional irradiation-induced effects such as surface sputtering become important. In this paper, we present results from 340 keV Xe^{++} irradiations of yttria-stabilized zirconia (YSZ) to fluences ranging from 1×10^{15} to 1.5×10^{21} ions/m^2. No amorphization of YSZ was observed after irradiation to even the highest ion fluence. To assess sputtering effects at high fluence, an analytical model was developed, using ion range and damage distributions calculated using Monte Carlo simulations for ion–solid interactions. Analysis results and experimental data revealed that at high fluences, the implanted ion and damage distribution profiles are significantly modified by sputtering.

1. Introduction

Fully stabilized zirconia has been proposed for use in non-uranium-bearing, proliferation resistant fuels that incorporate plutonium and burnable poisons in neutronically inert and chemically durable matrices [1,2]. Actinides are readily incorporated into the zirconia structure. Cubic zirconia is isostructural with PuO_2 and UO_2.

Many ion irradiation experiments have shown that cubic-stabilized zirconia is highly resistant to radiation-induced amorphization (see Table 1 and Refs. [3–10]). But due to cubic zirconia's high amorphization resistance, irradiation experiments to very high ion fluences are required to assess its radiation tolerance. At high ion fluence, additional irradiation-induced effects such as surface sputtering become important.

During ion irradiation, some material at the surface of an implanted sample is sputtered. At low doses of irradiation, this effect does not produce significant changes in the ion distribution and damage profiles. However, at higher doses sputtering can remove significant amounts of target material as well as previously implanted ions. Eventually, an equilibrium condition (steady state) may be reached, wherein as many implanted atoms are removed by sputtering as are replenished by implantation. The same is true of ion-beam induced displacement damage: previously existing damage can be removed at the same rate as new damage is introduced. In previous ion irradiation studies on cubic zirconia, effects due to sputtering were neglected.

To account for sputtering effects on implanted ions profiles, various models have been proposed. Analytical treatments of the interaction between primary ions and a surface have been proposed (for example, see [11,12]), as well as Monte Carlo simulations with dynamically

* Corresponding author. Tel.: +1-505 665 3457; fax: +1-505 667 6802.

E-mail address: kurt@lanl.gov (K.E. Sickafus).

0022-3115/02/$ - see front matter
PII: S0022-3115(02)01233-3

Table 1
Ion irradiation damage studies of cubic, YSZ

Type of ions and energy	Maximum fluence (ion/m^2)	Displacements per atom by author	Displacements per atom calculated taking into account sputtering	Amorphization	Reference
240 keV Xe^+	1×10^{21}	–		No	[3]
160 keV Pt^+	5×10^{20}	–		No	[4]
400 keV Xe^{++}	3×10^{20}	110		No	[5]
60 keV Xe^+	1.8×10^{20}	–		No	[1]
1.5 MeV Xe^+	1.8×10^{20}			No	
72 MeV I^+	5×10^{19}	7.7		No	[6]
400 keV Xe^{++}	3×10^{20}	–		No	[7]
60 keV Xe^{2+}	1.8×10^{20}	–		No	[8]
340–400 keV Xe^{++},	3×10^{20}	100		No	[9]
72 MeV I^+	5×10^{19}	7.7		No	
400 keV Cs^+	1×10^{21}	330	195	Yes	[10]
70 keV Cs^+	1×10^{21}				
340 keV Xe^{++}	1×10^{21}		177	No (polygonization)	This study

varying target compositions [13–16]. Detailed reviews of models for ion implantation in the presence of sputtering can be found elsewhere [17,18].

In this study, we developed an analytical model for analysis of effects due to sputtering on implanted ion distributions as well as damage profiles. We complemented our analysis with ion–solid interaction simulations based on the Monte Carlo program SRIM by Ziegler et al. [19]. The results show that sputtering significantly alters the profile of implanted ions, as well as the maximum damage produced in the implanted material. At high fluences, neglecting sputtering leads to an overestimation of both the implanted ion concentration and the peak displacement damage.

In earlier analytical models used to describe the sorption of gas during ions bombardment of solid surfaces it was shown that the shape of implanted ion and damage distribution can be significantly altered due to the sputtering taking place during ion irradiation [11]. The proposed theoretical models were somewhat difficult to use because they assumed a general shape for the probability of an ion to stop at a given depth and for the probability to create damage. In this study, we developed a simple model that is relevant to a large class of radiation damage experiments. Specifically, our model can be applied to any material irradiated with heavy ions. The model proposed here provides a simple means to estimate the effect of sputtering in ion irradiation experiments of nuclear materials using readily available methods, such as Rutherford backscattering spectroscopy and channeling (RBS/C) combined with Monte Carlo simulations. Our results are consistent with general models.

2. Experimental procedure

(1 0 0)-oriented cubic-stabilized zirconia single crystals, obtained from Zirmat Corp., were used in this study. The zirconia crystals contained 9.5 mol.% Y_2O_3, heretofore to be referred to as yttria-stabilized zirconia (YSZ). The crystals were 0.5 mm thick and polished on both sides.

YSZ single crystals were irradiated with 340 keV Xe^{++} ions using a 200 kV ion implanter in the Ion-Beam Materials Laboratory (IBML) at Los Alamos National Laboratory. Ion fluences ranged from 1×10^{15} to 1.5×10^{21} ions/m^2. The ion flux was 5×10^{14} ions/m^2 s for fluence 1×10^{15} ions/m^2; the flux was $5–9 \times 10^{15}$ ions/m^2 s for fluences $1 \times 10^{16}–1 \times 10^{19}$ ions/m^2; and the flux was 1×10^{17} ions/m^2 s for fluences $1 \times 10^{20}–1.5 \times 10^{21}$ ions/m^2. Samples were tilted about 6° for irradiation to minimize ion-channeling effects during irradiation. The sample stage was cooled to 100 K by liquid nitrogen conduction cooling. After implantation, the samples were warmed to room temperature for measurements. Calculations of ion range and energy deposition were made using the Monte Carlo code SRIM-2000 (version 2000-39) by Ziegler et al. [19]. For these calculations, we used a density of 5.96 g/cm^3 for YSZ (from JCPDS file 30-1468) [20], for composition $Zr_{0.85}Y_{0.15}O_{1.93}$, close to the composition of our samples. A threshold displacement energy of 40 eV was used for all target elements. This choice is arbitrary and has often been used in previous studies [5].

Rutherford backscattering spectroscopy and ion-channeling (RBS/C) were used to analyze the radiation-induced damage accumulation following ion irradiation.

For RBS/C, an analyzing beam of 2.0 MeV helium, oriented normal to the sample, was used. The detector was located 13° off-axis relative to the incident beam direction. The RBS/C measurements were performed ex situ at room temperature.

Implanted microstructures were examined using transmission electron microscopy (TEM) on samples prepared in cross-sectional geometry. TEM observations were made using a Philips CM-30 electron microscope operating at 300 kV.

3. Experimental results

RBS/C spectra in Fig. 1 show the progression of damage accumulation in zirconia with increasing Xe ion dose. A subsurface damage peak is apparent at low doses (for example, at an ion fluence of 1×10^{19} ions/m^2). This peak broadens with increasing dose until it meets the surface scattering position. The height of the damage peak also rises with increasing dose. However, this increase is partially due to overlap with the implanted Xe peak and the Zr surface scattering peak. To overcome this interference between scattering (of He ions) by implanted Xe ions versus scattering from the damage layer, we selected a set of channels (600–630) below the Zr surface scattering position, and estimated damage by integrating the He backscattered yield within this energy window. We define a damage accumulation parameter, χ, as the ratio of the integral obtained over this energy window with the crystal oriented for channeling, versus the integral over the same window when the crystal is 'randomly' oriented. Using this method, we determined that χ increases with increasing Xe dose and saturates at a value of 1 at fluence 1×10^{21} ions/m^2. A value $\chi = 1$ may be interpreted as due to the formation of either an amorphous or a polycrystalline layer at the surface of zirconia samples. Fleischer et al. [3] did not observe saturation at $\chi = 1$, although they used a large fluence, 1×10^{21} Xe/m^2. However, in their case, the energy of the Xe ions was lower (240 keV).

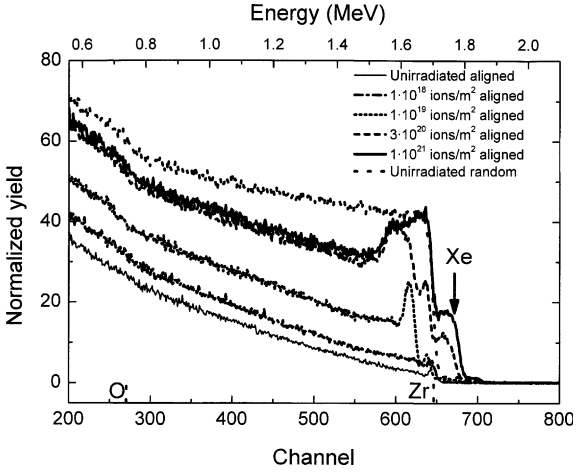

Fig. 1. Ion channeling spectra obtained from YSZ single crystals irradiated with 340 keV Xe ions at 100 K to the fluences indicated.

It is interesting to observe that in RBS spectra obtained from Xe implanted zirconia, the Xe peak has the same magnitude for fluences 1×10^{21} and 1.5×10^{21} ions/m^2. Using the RUMP RBS spectrum simulation program [21], we analyzed this peak and determined that the integrated intensity for the Xe peaks in these spectra corresponds to an areal atom density (heretofore referred to as the projected ion concentration) of 5×10^{20} ions/m^2. This saturation in the Xe concentration is due to the concurrent process of surface sputtering. Similarly, in the experimental results published by Fleischer et al. [3], the measured Xe concentration reached a limiting value at fluences greater than 3×10^{20} ions/m^2. Fleischer et al. used lower energy (240 keV) Xe ions than we used in our experiment, so results from these two studies are quite consistent.

Fig. 2 shows a bright field TEM image obtained from a YSZ irradiated sample with 340 keV Xe ions to a fluence of 1×10^{21} ions/m^2. The damaged layer extends to the depth of approximately 170 nm. One can see voids or bubbles formed by accumulated xenon. Microdiffraction patterns of the damaged layer and the substrate are shown as insets in Fig. 2 (labeled 1 and 2, respectively). The diffraction pattern from the damaged layer shows no evidence for amorphization of the irradiated layer. The pattern exhibits similarities to the pattern obtained from the substrate. Extra reflections are due to a polygonized microstructure. These results indicate that no phase transformation occurs in YSZ after high dose, heavy ion irradiation. Similar results were obtained by Matzke et al. in UO_2 irradiated with 300 keV Xe ions [22]. In their samples, polygonization had occurred causing a fine-grained polycrystalline structure with a misalignment between grains of only a few degrees. They also observed saturation of Xe concentration at high ion fluences.

4. Computational analysis

For our analysis, we used a receding surface model similar to the one developed by Carter [11,12]. We made the following assumptions: (1) both the implanted ion range and displacement damage distribution can be represented by Gaussian distributions; (2) implanted ions do not alter the target atom density significantly; (3) implanted ions have about the same sputtering yield as an average target atom; and (4) the sticking probability (i.e., the probability that an incident ion will be adsorbed or absorbed by the solid) is unity. We used

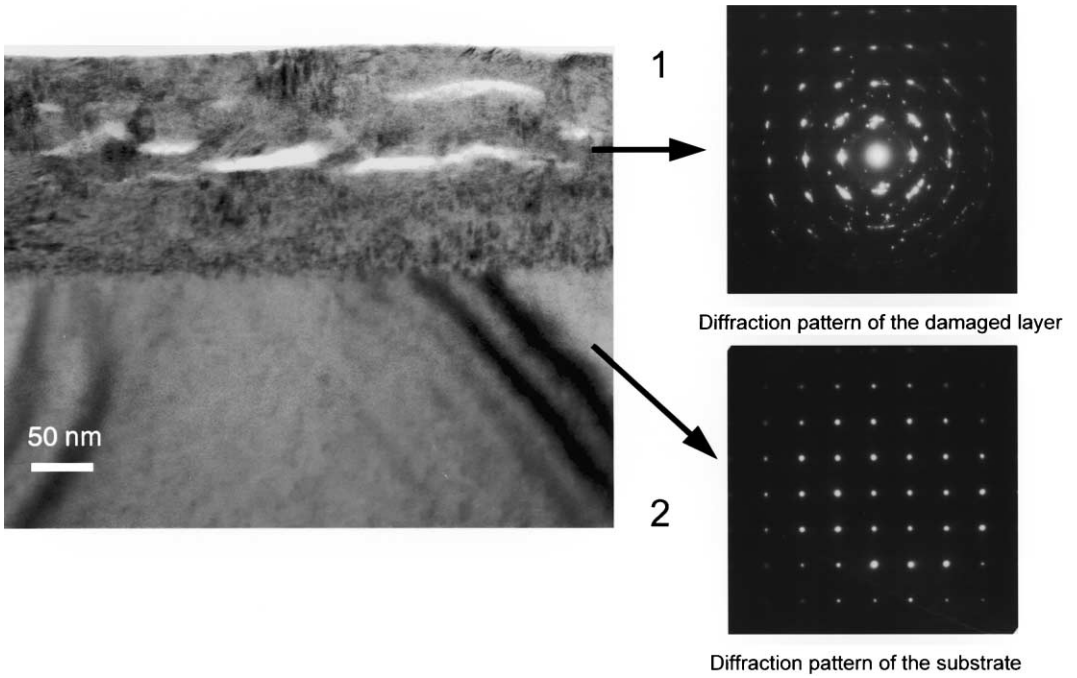

Fig. 2. Bright-field transmission electron micrograph from an YSZ single crystal irradiated with 340 keV Xe^{++} ions to a fluence of 1×10^{21} ions/m^2. Region 1 represents the damaged layer. Region 2 is the unirradiated zirconia substrate. The electron micro-diffraction patterns at the right were obtained from the damaged layer (top) and the substrate (bottom).

Monte Carlo simulations (SRIM) to calculate the depth distribution of Xe ions implanted into YSZ as well as the depth distribution of the displacement damage. The SRIM-calculated concentration versus depth profile for 340 keV Xe ions implanted into YSZ is well characterized by a Gaussian distribution centered near the mean projected range. Fig. 3 shows this ion implantation profile, along with a Gaussian fit to the simulation results. The implanted ion distribution can also be interpreted as the probability for one ion to stop at a specific depth x. This probability can be written as

$$\rho_1(x) = \frac{1}{\sigma\sqrt{2\pi}} \exp - \frac{(x - x_0)^2}{2\sigma^2}, \quad (1)$$

where x_0 is the position of the center of the peak; σ is the standard deviation of the Gaussian distribution (σ is approximately 0.425 of the full width of the ion distribution peak at half height and is equivalent to the longitudinal straggling of the ion distribution). The values for x_0 and σ obtained from the Gaussian fit to the SRIM simulation are $x_0 = 72$ nm, $\sigma = 26.2$ nm.

At high fluences, sputtering can significantly alter the concentration profile and so, the maximum attainable implanted ion concentration. For the case of no sputtering, an incremental increase in ion fluence, $\Delta\Phi$, produces a corresponding increase in concentration of implanted atoms, $\Delta\rho_i$, which, assuming a Gaussian depth distribution, is given by

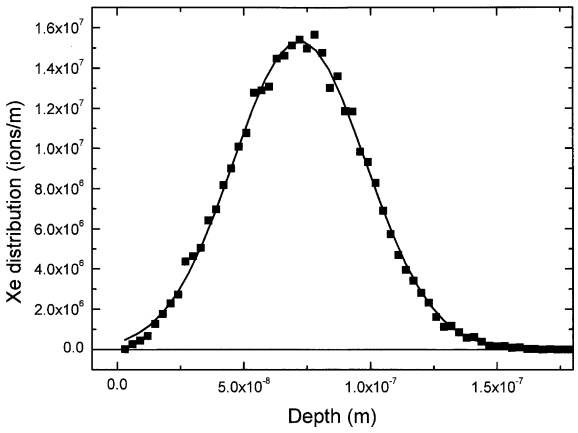

Fig. 3. Probability distribution for a 340 keV Xe^{++} ion implanted into YSZ to stop at a given depth in the target. Squares: SRIM calculation. Line: Gaussian fit to SRIM simulation.

$$\Delta\rho_i(x)\ [\text{atoms/m}^3] = \Delta\Phi\ [\text{ions/m}^2] \frac{1}{\sigma\sqrt{2\pi}} \times \exp\left(-\frac{(x - x_0)^2}{2\sigma^2}\right)\ [\text{m}^{-1}]. \quad (2)$$

With sputtering, the sample surface erodes with increasing fluence at a constant rate given by

$$\frac{\Delta x}{\Delta \Phi}\,\frac{[\mathrm{m}]}{[\mathrm{ions/m^2}]} = \frac{k}{\rho_t}\,\frac{[\mathrm{atoms/ion}]}{[\mathrm{atoms/m^3}]}, \tag{3}$$

where k the sputtering yield (atoms/ion) and ρ_t the atomic density of target (atoms/m^3). Eq. (3) implies that if k is non-zero, then the depth scale (x) for the target must change during irradiation. $\Delta x/\Delta\Phi$ is the 'velocity' of the coordinate system attached to the moving target surface (x'), relative to a stationary coordinate system (x) associated with the target surface at $\Phi = 0$ (Fig. 4). Consequently, an arbitrary depth into the sample, x', in the moving reference frame at fluence Φ is related to depth x in the $\Phi = 0$ fixed coordinate system by

$$x' = x - \frac{\Delta x}{\Delta \Phi}\Delta\Phi = x - \frac{k}{\rho_t}\Phi, \tag{4}$$

since $\Delta\Phi = \Phi - 0$. Take, for instance, the mean depth of implanted atoms at $\Phi = 0$, i.e., x_0, upon irradiation to a final ion fluence, Φ_f. According to Eq. (4), this occurs at a reduced depth given by

$$x_0' = x_0 - \frac{\Delta x}{\Delta \Phi}\Delta\Phi = x_0 - \frac{k}{\rho_t}\Phi_f, \tag{5}$$

since $\Delta\Phi = \Phi_f - 0$. The mean depth of implanted atoms for intermediate fluences between $\Phi = 0$ and $\Phi = \Phi_f$ occurs at smaller reduced depths relative to the final depth scale:

$$x_0^{\Phi} = x_0 - \frac{k}{\rho_t}(\Phi_f - \Phi). \tag{6}$$

We desire to calculate the final concentration of implanted atoms with respect to the final depth scale, x'. By analogy to Eq. (2), we can write for the concentration profile associated with incremental fluence $\Delta\Phi$ about Φ:

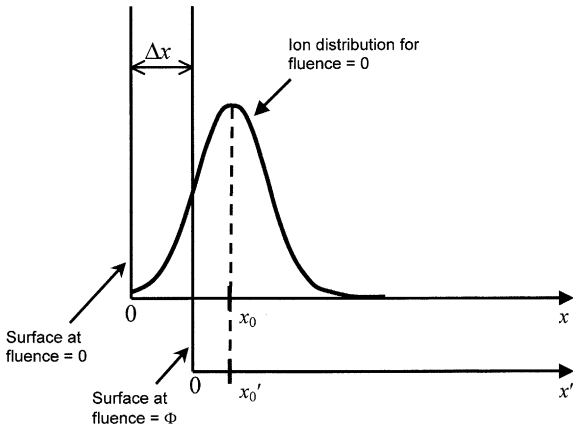

Fig. 4. Schematic drawing of surface erosion due to sputtering under ion irradiation.

$$\Delta\rho_i(x') = \frac{\Delta\Phi}{\sigma\sqrt{2\pi}}\exp\left(-\frac{(x' - x_0^{\Phi})^2}{2\sigma^2}\right). \tag{7}$$

Substituting x_0^{Φ} (Eq. (6)) into Eq. (7) and integrating with respect to fluence to Φ_f, the final implanted concentration profile is obtained:

$$\rho_i(x') = \frac{1}{\sigma\sqrt{2\pi}}\int_0^{\Phi_f} d\Phi \exp\left(-\frac{\left(x' - x_0 + \frac{k}{\rho_t}(\Phi_f - \Phi)\right)^2}{2\sigma^2}\right). \tag{8}$$

This integral has a simple analytical solution given by

$$\rho_i(x') = \frac{\rho_t}{2k}\left(-\mathrm{Erf}\left[\frac{x' - x_0}{\sqrt{2}\sigma}\right] + \mathrm{Erf}\left[\frac{x'\rho_t - x_0\rho_t + k\Phi_f}{\sqrt{2}\rho_t\sigma}\right]\right). \tag{9}$$

Integrating Eq. (9) with respect to x' from $-\infty$ to $+\infty$ yields the final incident ion fluence, Φ_f (ions/m^2), whereas integration from a lower limit $x' = 0$ yields an expression for the total retained ion concentration, $N(\Phi_f)$ (this is a projected ion concentration in units of (ions/m^2)):

$$N(\Phi_f)\ [\mathrm{ions/m^2}] = \int_0^{\infty} dx'\,\rho_i(x'). \tag{10}$$

Fig. 5 shows the dependence of the total retained implantation concentration $N(\Phi_f)$ on sputtering yield for selected irradiation fluences (Φ_f). These results were obtained using Eq. (10) along with the values of x_0 and σ obtained from fitting SRIM results with a Gaussian curve (Eq. (1)). As expected, in the absence of sputtering ($k = 0$), the retained ion concentration is equal to the total irradiation fluence. However, with increasing sputtering yield ($k > 0$), N begins to differ significantly from the irradiation fluence. In our RBS/C experiment, we found that the retained concentration of Xe ions after irradiation to fluences of 1×10^{21} and 1.5×10^{21} ions/m^2 was equal to 5×10^{20} ions/m^2. From results shown in Fig. 5, we find that this retained ion concentration corresponds to a sputtering yield of about 12 atoms/ion.

Based on this sputtering yield, $k = 12$, Fig. 6 shows the calculated retained projected ion concentration $N(\Phi_f)$ (from Eq. (10)) for irradiation of YSZ with 340 keV Xe ions, versus the delivered ion concentration (Φ_f). One can see that at fluences up to 1×10^{20} ions/m^2, the retained concentration of Xe ions is not influenced by the sputtering process. However, at a fluence of 3×10^{20} ions/m^2, a difference between the delivered ($k = 0$) versus the retained ($k = 12$) concentration of Xe ions becomes apparent. The concentration of implanted Xe ions

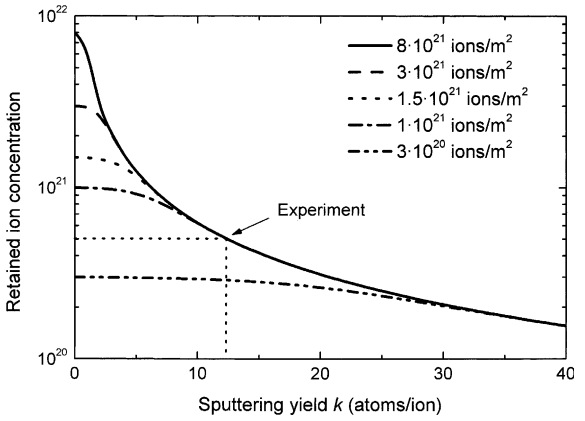

Fig. 5. Calculated dependence of the retained, depth-integrated ion concentration $N(\Phi_f)$ on the sputtering yield (k) for selected ion fluences (Φ_f) (obtained using Eq. (10)).

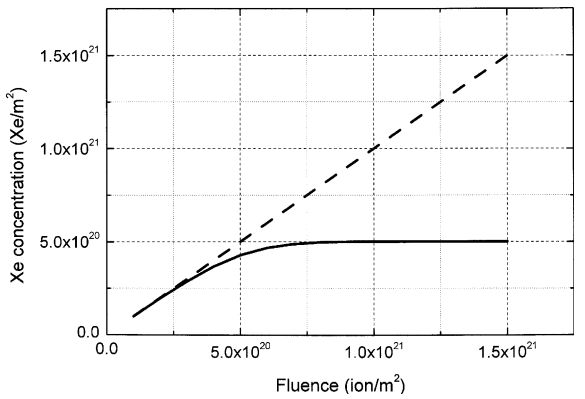

Fig. 6. Comparison of delivered (Φ_f) and retained N number of ions per unit surface area, assuming a sputtering yield $k = 12$. The solid line represents the retained Xe concentration integrated over the sample depth (obtained using Eq. (10). The dashed line represents the delivered ion fluence (equivalent to $k = 0$).

reaches saturation by a fluence of 1×10^{21} ions/m^2. Similar changes in the profile of implanted ions was obtained by Carter [12] in his numerical calculations. The 'saturation' effect in ion implantation was first published by Nielsen [23].

Fig. 7 shows Xe ion depth profiles for selected ion fluences, based on calculations using Eqs. (8,9) and using the sputtering yield, $k = 12$. If no account is taken for sputtering, the calculated peak Xe concentration in YSZ after irradiation to 1×10^{21} ions/m^2 is equal to about 18 at.% Xe. However, due to removal of surface material containing both YSZ target atoms and previously implanted Xe ions, the distribution and concentration of Xe ions is altered. For irradiation fluences below 1×10^{20} ions/m^2, the shape of the ion implantation profile remains approximately unchanged and has a

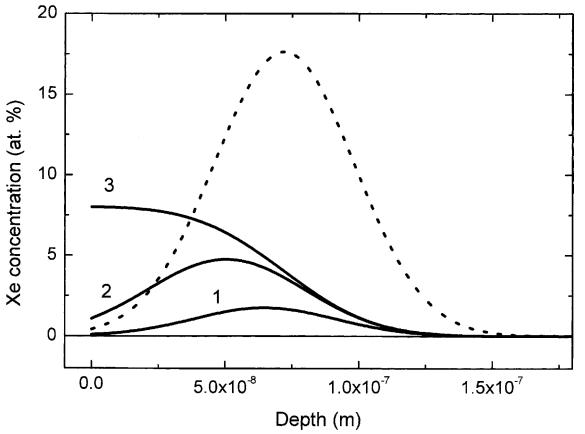

Fig. 7. Xe-ion distribution profiles. The dotted line represents the ion profile for fluence 1×10^{21} ions/m^2 and for sputtering yield $k = 0$. Solid lines represent simulated ion profiles for different fluences with sputtering yield $k = 12$: (1) 1×10^{20} ions/m^2, (2) 3×10^{20} ions/m^2, and (3) 1×10^{21} ions/m^2 (obtained using Eq. (9)).

bell-like shape (Fig. 7). However, at higher fluences the shape of the distribution changes significantly. At fluences where the sputtering and deposition rates reach equilibrium, the curve has a maximum at the surface of the target and concentration decreases with depth into the target (Fig. 7).

The same type of analysis can be applied to the displacement damage distribution. The output of the SRIM code yields the damage distribution in units of (vacancies/m ion). As in the case of the ion implantation profile, this distribution is also described satisfactorily by a Gaussian curve (Fig. 8). This distribution is equivalent to the probability of finding vacancies as a function of depth into the target (units: vacancies/m ion) and can be written as

$$\rho_{\mathrm{vac}}(x) = \frac{A}{\sigma_{\mathrm{vac}}\sqrt{2\pi}} \exp\left(-\frac{(x - x_{0\mathrm{vac}})^2}{2\sigma_{\mathrm{vac}}^2}\right), \tag{11}$$

where A is a mean number of vacancies produced by a single ion; $x_{0\mathrm{vac}}$ is the position of the center of the vacancy depth distribution profile; σ_{vac} is the standard deviation of the Gaussian distribution. By analogy with Eq. (8), the calculated distribution of the displacement damage (units: displacements per atom or dpa) can be written as

$$\rho_{\mathrm{vac}}(x, \Phi) = \frac{A}{\rho_t \sigma_{\mathrm{vac}}\sqrt{2\pi}} \int_0^{\Phi_f} \mathrm{d}\Phi \times \exp\left(-\frac{\left(x' - x_0 + \frac{k}{\rho_t}(\Phi_f - \Phi)\right)^2}{2\sigma_{\mathrm{vac}}^2}\right), \tag{12}$$

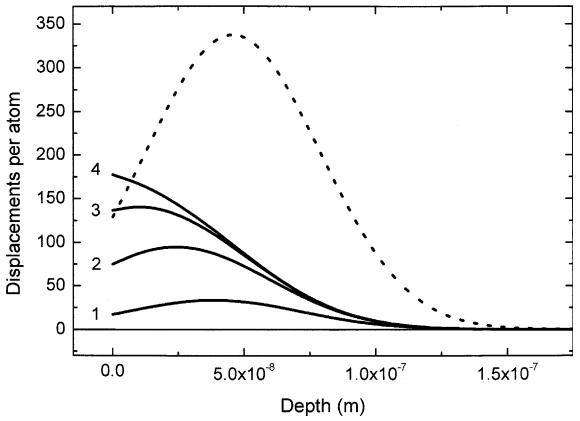

Fig. 8. Damage distribution profiles. The dotted line represents the damage profile for the fluence of 1×10^{21} ions/m^2, using a sputtering yield $k = 0$. Solid lines represent simulated ion profiles for different fluences using a sputtering yield, $k = 12$: (1) 1×10^{20} ions/m^2, (2) 3×10^{20} ions/m^2, (3) 5×10^{20} ions/m^2, and (4) 1×10^{21} ions/m^2 (obtained using Eq. (12)).

where ρ_t is the target density (units: atoms/m^3). Since we do not know exact values for the displacement energies and lattice binding energies of the target atoms, the calculated number of displacements per atom is merely an estimation. Nevertheless, the calculations indicate trends in displacement damage profile alterations with increasing ion fluence.

Fig. 8 shows calculated damage profiles for 340 keV Xe ions irradiation of YSZ to selected fluences, based on Eq. (12). As in the case of ion implantation distributions shown earlier, with higher fluences damage profiles change significantly. The damage calculated without taking into account the sputtering process is much higher than the damage obtained upon reaching equilibrium between creation of new defects and their removal due to sputtering. According to our calculations, the maximum retained damage is about 180 dpa. Fig. 8 also shows the damage profile calculated without taking into account the sputtering process. One can see that this profile gives an overestimation for damage produced in the material as well as an incorrect shape for the damage distribution.

These results are only approximate due to differences between the extent of the calculated ion damage profiles versus the damage profiles observed in cross-sectional TEM images. In actual radiation damage experiments, the projected ion range is found to be greater than that of the calculated range. Similar results, wherein the measured ion range exceeded the calculated range, were found for 60 keV Xe^{2+} ions by Sasajima et al. [8]. However, the results presented here clearly indicate that for high dose ion irradiation experiments, actual ion distribution and damage profiles can be significantly different compared to the calculated profiles. Sputtering effects should not be neglected under high dose irradiation conditions.

It should be noted that the SRIM code also calculates a sputtering yield, that depends sensitively on the assumed surface binding energies for the target atoms. We performed SRIM simulations using the default surface binding energies for Zr, Y, and O atoms provided by SRIM, and found that these energies must be reduced by approximately a factor of 2 in order to correspond with our experimental and computational analysis results.

5. Discussion

Sputtering may have important implications regarding the interpretation of other ion irradiation experiments. For instance, Fleischer et al. [3] performed 240 keV Xe irradiations of YSZ and observed a saturation of the projected Xe concentration at high ion fluence. Based on their RBS data, the projected Xe concentration for 240 keV Xe saturates for ion fluences greater than 3×10^{20} ions/m^2. Using our computational analysis procedure and a sputtering yield for 240 keV Xe ions similar to the 340 keV value ($k = 12$), we found a saturation in the projected Xe concentration ($N = 3.5 \times 10^{20}$ ions/m^2) in reasonable agreement with their measured value.

In another study, Wang et al. [10] used 400 keV Cs ions to irradiate YSZ at room temperature and observed an amorphization transformation at high ion dose (they speculated that amorphization occurs because monovalent Cs ions, which possess a relatively large ionic radius, disrupt the local atomic configurations in cubic YSZ). We performed a sputtering analysis for their experimental conditions to assess the importance of sputtering effects in their experiment. Wang et al. show cross-sectional TEM microstructural observations (Fig. 2 of Ref. [10]) for Cs^+ irradiation of YSZ to a fluence of 1×10^{21} ions/m^2. In this figure, a Cs atomic concentration profile is superimposed on the irradiated sample microstructure (results based on analytical TEM measurements, normalized using a SRIM simulation; it should also be noted that the figure caption indicates the ion energy used was 70 keV, but the ion depth distribution apparent in the figure suggests that the micrograph was obtained from a 400 keV Cs^+ irradiated sample). The measured Cs concentration profile is bell-shaped with the Cs concentration at the surface equal to almost zero. But using the computational analysis procedure discussed here, this result is not easily rationalized for the high Cs^+ fluence of 1×10^{21} ions/m^2. Assuming a sputtering yield similar to that for 340 keV Xe^{++} ions ($k = 12$), we simulated Cs concentration and retained damage profiles for 400 keV Cs^+ ion irradiation of YSZ. At a fluence of 1×10^{21} ions/m^2, we found that the maximum retained projected Cs concentration was approximately

$N = 5.7 \times 10^{20}$ ions/m^2. Both the implanted Cs ion concentration and the damage profiles are maximum at the target surface for this ion dose. According to our calculations, the peak displacement damage (at the target surface) is approximately 200 dpa. The observed buried amorphous layer and the minimally damaged surface layer (Fig. 2 of Ref. [10]), as well as the bell-shaped Cs concentration profile, suggest that 400 keV Cs^+ ions have an extremely low sputtering yield in YSZ. This could be tested by considering the results shown graphically in Fig. 4 of this paper. If $k \simeq 0$ for the described irradiation conditions, then the projected implanted ion concentration should not exhibit saturation with increasing ion fluence. However, this is not probable, when one considers results of sputtering experiments such as those performed by Almén and Bruce [24]. These authors measured sputtering effects for many beams and targets. One of their findings was that there is little difference in sputtering between Xe and Cs in many targets. This suggests that the results obtained by Wang et al. [10] are probably in error. It should be also noted that Hocking et al. [25] showed that there was a clear redistribution of Cs occurring during implantation into UO_2. The redistribution increased Cs concentration in the near surface layer.

It should be noted, as first reported by Brown and Davies [26], that the sputtering alone cannot explain many observed implantation profiles. They demonstrated that range profiles and saturation are due to a complex equilibrium between sputtering, scattering, knock-on, and crystal lattice effects.

6. Conclusions

Experimental TEM results indicate that irradiation of YSZ with 340 keV Xe^{++} ions does not produce amorphization of this material. The TEM results indicate that the highest dose Xe ion irradiation produces a partially polygonized microstructure in YSZ. RBS measurements revealed that the projected concentration of implanted Xe ions reaches saturation at a value of about 5×10^{20} ions/m^2. It is assumed in this study that this saturation in the implanted ion concentration is due to sputtering, which leads to a limit on the maximum concentration of Xe atoms that can be retained in the target material.

A simple analytical model, combined with Monte Carlo (SRIM) simulations and RBS measurements of implanted ion concentrations, was used to assess sputtering effects in heavy ion irradiated YSZ. From this analysis, the sputtering yield for the ion irradiation conditions used in this investigation was found to be $k = 12$. For Xe fluences exceeding 3×10^{20} ions/m^2, computational results based on this sputtering yield indicate that the concentration of implanted Xe ions differs significantly from the number of ions delivered to the target. An equilibrium is established by a fluence of 1×10^{21} ions/m^2, in which the Xe projected ion concentration saturates at 5×10^{20} ions/m^2. Irradiation to higher fluences does not produce any significant changes in the material. The shape of the ion distribution is no longer bell-like, but exhibits a maximum at the target surface. The corresponding peak displacement damage occurs at the surface of the target and saturates at a value of about 180 dpa.

Acknowledgements

The authors wish to thank J.R. Tesmer, C.J. Maggiore, C.R. Evans, and M.G. Hollander for help with ion irradiation and analysis assistance; and F. Li and R.M. Dickerson for help with TEM measurements. This research was sponsored by the US Department of Energy, Office of Basic Energy Sciences, Division of Materials Sciences.

References

[1] C. Degueldre, J.M. Paratte, Nucl. Technol. 123 (1998) 21.
[2] Hj. Matzke, V.V. Rondinella, T. Wiss, J. Nucl. Mater. 274 (1999) 47.
[3] E.L. Fleischer, M.G. Norton, M.A. Zaleski, W. Hertl, C.B. Carter, J.W. Mayer, J. Mater. Res. 6 (1991) 1905.
[4] D.Z. Xie, D.Z. Zhu, D.X. Cao, Z.Y. Zhou, Nucl. Instrum. and Meth. B 132 (1997) 425.
[5] N. Yu, K.E. Sickafus, P. Kodali, M. Nastasi, J. Nucl. Mater. 244 (1997) 266.
[6] K.E. Sickafus, Hj. Matzke, K. Yasuda, P. Chodak, R.A. Verrall, P.G. Lucuta, H.R. Andrews, A. Turos, R. Fromknecht, N.P. Baker, Nucl. Instrum. and Meth. B 141 (1998) 358.
[7] K. Yasuda, M. Nastasi, K.E. Sickafus, C.J. Maggiore, N. Yu, Nucl. Instrum. and Meth. B 138 (1998) 499.
[8] N. Sasajima, T. Matsui, K. Hojou, S. Furuno, H. Otsu, K. Izui, T. Muromura, Nucl. Instrum. and Meth. B 141 (1998) 487.
[9] K.E. Sickafus, Hj. Matzke, T. Hartmann, K. Yasuda, J.A. Valdez, P. Chodak, M. Nastasi, R.A. Verrall, J. Nucl. Mater. 274 (1999) 66.
[10] L.M. Wang, S.X. Wang, R.C. Ewing, Philos. Mag. Lett. 80 (2000) 341.
[11] G. Carter, J.S. Colligon, J.H. Leck, Proc. Phys. Soc. 79 (1962) 299.
[12] G. Carter, R. Webb, R. Collins, Radiat. Eff. 37 (1978) 21.
[13] M.L. Roush, T.D. Andreadis, O.F. Goktepe, Radiat. Eff. Def. Solid 55 (1981) 119.
[14] W. Möller, W. Eckstein, Nucl. Instrum. and Meth. B 230 (1984) 814.
[15] A. Schonborn, N. Hecking, E.H. Tekaat, Nucl. Instrum. and Meth. B 43 (1989) 170.
[16] Y. Miyagawa, M. Ikeyama, K. Saito, G. Massouras, S. Miyagawa, J. Appl. Phys. 70 (1991) 7289.

[17] M. Nastasi, J.W. Mayer, J.K. Hirvonen, Ion–Solid Interactions: Fundamentals and Applications, Cambridge University Press, Cambridge, 1996.
[18] A. Galdikas, L. Praniavichius, in: Interaction of Ions with a Condensed Matter, vol. 229, Nova Science Publishers, New York, 2000.
[19] J.F. Ziegler, J.P. Biersack, U. Littmark, The Stopping and Range of Ions in Solids, Pergamon, New York, 1985.
[20] I.C.F.D. Data, Powder Diffraction File. Joint Committee on Powder Diffraction Standards, Philadelphia, PA, 1974 – present.
[21] L.R. Doolittle, Nucl. Instrum. and Meth. B 9 (1985) 344.
[22] Hj. Matzke, A. Turos, G. Linker, Nucl. Instrum. and Meth. B 91 (1994) 294.
[23] H.L. Nielsen, in: M.L. Smith (Ed.), Electromagnetically Enriched Isotopes and Mass Spectrometry Proceedings of the Conference Held in Cockcroft Hall, Harwell, 13–16 September 1955, Academic Press, NY, 1956, p. 68.
[24] O. Almén, G. Bruce, Nucl. Instrum. and Meth. 11 (1961) 257.
[25] W.H. Hocking, R.A. Verrall, P.G. Lucuta, Hj. Matzke, Radiat. Eff. Def. Solid 125 (1993) 299.
[26] F. Brown, J.A. Davies, Can. J. Phys. 41 (1963) 844.